etrieval of Object Information from Electron iffraction as Ill-Posed Inverse Problems

rt Scheerschmidt

Iax Planck Institute of Microstructure Physics
Veinberg2, D-06120 Halle, Germany
'hone: +49-345-5582910, Fax: +49-345-5511223
:mail: schee@mpi-msp-halle.mpg.de

stract. Inverse problems as direct solutions of electron scattering equations can be luced using either an invertible linearized eigenvalue system or a discretized form the diffraction equations. The analysis is based on the knowledge of the complex :tron wave at the exit plane of an object reconstructed for single reflections by :tron holography or other wave reconstruction techniques. In principle, this enables direct retrieval of the local thickness and orientation of a sample as well as the nement of potential coefficients or the determination of the atomic displacements, ısed by a crystal lattice defect, relative to the atom positions of the perfect lat-e. Considering the sample orientation as perturbation the solution is given by a ıeralized and regularized Moore-Penrose inverse. Extracting solely the atomic dis-cements the latter are given by the zeros of a function with an incompletely known ırier spectrum. The numerical algorithms resulting from the fundamental relations ply ill-posed inverse problems.

Introduction

verse problems are difficult, always fascinating, and in most of the cases ill improperly posed (Tichinov and Arsenin (1977), Lavrentiev (1967)). Ill or properly posed means that one or all requirements are violated that usually aracterize physics, i.e. existence, uniqueness and stability of a solution. As :en occurring in many physical investigations, in the mathematical sense, the :ect solution of the diffraction equations implies an inverse problem. Although e inverse problems violate especially the existence of unique and continuous lutions to arbitrary data they are of great practical importance, if the trial-d-error solution demands a large variety of possible solutions and models to be sted, mostly providing a better insight into the basic relations of the physical ıenomena.

For instance, the imaging of crystal defects by high-resolution transmission :ctron microscopy or with the help of electron diffraction contrast technique well known and routinely used. Though the theoretical image calculations ways tend to establish standard rules of interpretation, a direct and phe-›menological analysis of electron micrographs is mostly not possible, thus re-ıiring the application of image simulation and matching techniques. Images are odelled by calculating both the interaction process of the electron beam with

the almost periodic potential of the matter, and the subsequent Fourier imaging process including the microscope aberrations. The images calculated are fitted to the experiment by varying the defect model and the free parameters. This trial-and-error image matching technique is the indirect solution to the direct scattering problem applied to analyse the defect nature under investigation.

Electron holography or other reconstruction techniques (Lichte (1986), Lichte (1992), Coene et al. (1992), van Dyck et al.(1993)) permit the determination of the scattered wave function at the exit surface of the crystal directly out of the hologram or from defocus series up to the microscope information limit owing to the noise in the phase distortion. Especially the sidebands of a Fourier-transformed hologram represent the Fourier spectrum of the complete complex image wave and its conjugate, respectively, from which the object wave can be reconstructed. Thus, both the reconstructed amplitudes and phases can be compared to trial-and-error calculations (Lichte (1991), Lichte et al. (1992)).

In previous papers (Scheerschmidt and Hillebrand (1991), Scheerschmidt and Knoll (1994), Scheerschmidt and Knoll (1995a), Scheerschmidt and Knoll (1995b), Scheerschmidt (1997)) it was demonstrated that the local thickness and orientation can be calculated directly from the wave function reconstructed at the exit surface of the object instead of using trial-and-error simulation techniques. In principle, the analysis holds good also for the retrieval of the object potential, or if solely the positions of the atomic scattering centres are evaluated. The inverse problems, however, generally dealing with insufficiently measured data always require physically related information a priori. It was shown that the knowledge of both the amplitudes and phases of a sufficiently large number of plane waves scattered by the object as well as the partial knowledge of the potential of the perfect crystal structure imply the possibility of directly retrieving object information, instead of using trial-and-error simulation techniques. Two approximations are discussed to solve the resulting inverse scattering problem without reconstructing the whole crystal potential:

First, the special problem of retrieving the local sample orientation is solved on the basis of the perturbation approximation for perfect crystals, and by applying regularized and generalized matrices to invert the resulting linearized problem. The corresponding iteration procedure enables the direct analysis of the moduli and phases if a sufficient number of plane wave amplitudes can be separated yielding local thickness and bending of the object for each image pixel (Scheerschmidt and Knoll (1995b), Scheerschmidt (1997)).

Second, based on the knowledge of the reconstructed complex electron wave and using a discretized form of the diffraction equations, an alternative method is developed (Scheerschmidt and Knoll (1994), Scheerschmidt and Knoll (1995a)), yielding an algebraic equation system for the complex amplitudes and the elastic displacements. In principle, this system enables the direct retrieval of the atomic displacements, caused by a crystal lattice defect, relative to the atom positions of the perfect lattice. The equations are invertible provided the completeness of the plane waves is valid (continuity of the electron current). A special inverse problem of electron scattering is deduced considering solely those atomic dis-

cements given by the zeros of a function with an incompletely known Fourier ctrum from the scattered electron wave of which the displacement field of a stal lattice defect can, in principle, be retrieved.

The present paper outlines the fundamental relations for both special inverse blems describing some first numerical experiences related to the solution of direct retrieval of local thickness and orientation. Some numerical aspects considered as, e.g., the stability of unique inverse solutions in terms of noise, l the regularization of the problem.

Physical basis: Dynamical diffraction and holographic ive reconstruction

e HREM image contrast is mainly determined by two processes: First, by the tron diffraction owing to the interaction process of the electron beam with almost periodic potential of the matter and, second, by the interference of plane waves leaving the specimen and being transmitted by the microscope. suming that the object wave is reconstructed free of aberrations or under raction contrast conditions the influence of the microscope imaging process lf can be neglected. Thus the image contrast is solely determined by the raction of the electrons with the object potential.

The interaction of electrons with a crystalline object is described on the ba- of a periodic potential with the electron structure factors as the expansion fficients and the Bloch-wave method for solving the high-energy transmision tron diffraction. Different formulations can be given, using Bloch wave or ne wave representations of the scattered waves, applying direct or reciprocal ice expansion, and direct integration or slice techniques, which, in principle, equivalent descriptions (van Dyck (1985), Spence and Zuo (1992), van Dyck 89)). The object wave in terms of modified plane waves with complex ampli- les $\phi\mathbf{g}$ yields

$$o(R) = \sum_g \phi_g e^{2\pi i((\mathbf{k}+\mathbf{g})\mathbf{R}+\mathbf{s}\mathbf{g}\mathbf{t})} \tag{1}$$

with reflections $\mathbf{g}$, excitations $s\mathbf{g}$, wave vector $\mathbf{k}$, and thickness t of a parallel- ed object, $\mathbf{R} = (\mathbf{x}, \mathbf{y})$. The amplitudes $\phi\mathbf{g}$ are constant with respect to z in the uum outside the object, which means that the plane waves are the stationary utions of the wave equation. Within the crystal, however, the amplitudes of modified plane waves $\phi\mathbf{g}$ are z-dependent according to the Ewald pendulum ution as described by the Bloch waves, which are the stationary solution hin the periodic potential.

The basic equations of the Bloch wave presentation in forward scattering roximation are given by the eigenvalue system

$$\sum_{\mathbf{h}} A_{\mathbf{gh}} C_{\mathbf{h}} - \gamma C_{\mathbf{g}} = 0, \text{ with } 2k_z A_{\mathbf{gh}} = (2\mathbf{K}.\mathbf{g} - \mathbf{g}^2)\delta_{\mathbf{gh}} - \mathbf{V}_{\mathbf{g}-\mathbf{h}}, \tag{2}$$

yielding the amplitudes $C_{\mathbf{g}}{}^{(l)}$ of the l th partial wave and its "anpassung" $\gamma^{(l)}$ to the dispersion of the lattice as a function of the lattice potential (Fourier coefficient $V_{\mathbf{g}}$) as well as the relative orientation of the object with respect to the electron beam incidence $\mathbf{K}$. With these eigenvalues and vectors, for a plane parallel perfect crystal of thickness t the complex amplitudes $\phi_{\mathbf{g}}$ of eq. (1) are directly given in matrix form by

$$\Phi = CXC^{-1}\theta \tag{3}$$

where $\Phi = [\phi_{\mathbf{g}}]$ and θ are the vectors of the amplitudes of the exit and the incident waves, respectively, and $\mathbf{X}$ represents the diagonilized scattering matrix $e^{2\pi iAt}$.

Using furthermore the deformable ion approximation a crystal lattice defect can be included by its elastic displacement field $\mathbf{v}$ as a phase shift of the Fourier spectrum of the crystal potential. The evaluation of the quantum-theoretical scattering problem using the high-energy forward scattering approximation (see, e.g., (Anstis (1989), Howie and Basinski (1968)) for the derivation and the explicit form of the equations) yields a parabolic differential equation system for vector Φ of the complex amplitudes of the elastically scattered electron waves :

$$\partial\Phi/\partial z = (\Delta + V[e^{i\mathbf{gv}}])\Phi \tag{4}$$

with $\Delta = \{ik_z\nabla^2 - 2(\mathbf{k}+\mathbf{g})\nabla\}/2\mathbf{k'_z} + 2\pi(\mathbf{s_h} - \mathbf{s_g})\mathbf{z}$, $\nabla = (\partial/\partial x, \partial/\partial y, 0)$, $k'_z = k_z + g_z + s_{\mathbf{g}}$ and the potential V=V'+iV" including the lattice potential V' and the absorption V" (one electron-optical potential approximation of inelastic scattering) as well as the diagonal matrix of the defect phase shifts.

In addition, boundary and initial conditions have to be applied: The linearized high-energy approximation directly fits $\phi_{\mathbf{g}}(\mathbf{R}, \mathbf{t})$ at the crystal exit surface to $\phi_{\mathbf{g}}(\mathbf{R})$ outside, demanding $|\phi_{\mathbf{g}}(\mathbf{R}, \mathbf{0})| = \delta_{\mathbf{go}}$ at the entrance surface, whereas the continuity of the derivatives has to be omitted in the linearized case. It enables one, however, to estimate the unknown displacements at the exit foil surface by using eq. (4) without potential outside and inverting eq. (4) directly at the exit surface:

$$\{V[e^{i\mathbf{gv}}]\Phi = 2\Delta\Phi\}_{z=t} \tag{5}$$

Instead of boundary conditions one can assume a periodic continuation to describe large extended crystal slabs, i.e. $\phi_{\mathbf{g}}(x, y, z) = \phi_{\mathbf{g}}(x + X, y, z)$ and $\phi_{\mathbf{g}}(x, y, z) = \phi_{\mathbf{g}}(x, y + Y, z)$, with slab extensions X,Y approaching infinity.

Holography with electrons offers one of the possibilities of increasing the resolution by avoiding microscope aberrations. It also enables the complete complex object wave to be restored. Image plane off-axis holograms are recorded in a microscope which is equipped with a Möllenstedt-type electron biprism inserted between the back focal plane and the intermediate image plane of the objective lens (Lichte (1986), Lichte (1991), Lichte (1992), Lichte et al. (1992)). The object is arranged so that a reference wave outside of it is transferred through

microscope, and owing to a positive voltage of the biprism both waves mu-
lly overlap in the image plane creating additional interference fringes. The
nsity of the latter is modulated by the modulus of the object wave, whereas
fringe position is varied by the phase of the object wave. Thus the recorded
rference pattern is an electron hologram from which both the modulus and
phase of the object wave can be reconstructed by optical diffraction or nu-
ical reconstruction. The reconstruction starts with a Fourier transform of the
ogram. Besides two sidebands in the central region of the Fourier spectrum
zero peak and autocorrelation occur, which is equivalent to a conventional
ractogram. The sidebands represent the Fourier spectrum of the complete
plex image wave and its conjugate, respectively, from which the object wave
y) can thus be reconstructed by separating, centring, and applying the in-
se Fourier transform including a reciprocal Scherzer filter with damping and
roscope aberrations (Lichte (1991), Orchowski et al. (1995)).

In the following it is important that, besides the whole sideband, each single
ection of sufficient intensity can be reconstructed separately (Scheerschmidt
97)). This provides the possibility of noise reduction if suitable windows and
ring are applied and if the pixels are precisely centred to avoid additional
se shifts. The environment of the reflections included in the filtering process
to be chosen such that the information of local distortions folded with the
ections will be transferred to the reconstructed partial waves. The reconstruc-
n of the single reflections causes modulus and phase to be distributed in the
tial waves, which is the presupposition of the inverse algorithm discussed in
following.

Figure 1 demonstrates the wave and the single-reflex reconstruction using a
oretical hologram simulated for a Σ=13 (100) tilt grain boundary in gold,
ch is relaxed by molecular dynamics. Fig. 1(a) shows the simulated hologram,
l Fig.1(c), an enlarged region with the hologram fringes extending from the
tral part of the boundary, with the atomic columns around the interface. The
rier spectrum of the hologram is given in Fig.1(b), and the sideband selected
reconstruction in Fig.1(d), the pairs of the reflections are indicated with
corresponding reciprocal lattice vectors. Fig. 1(e) presents the reconstructed
l space intensities of the single reflections in amplitude (AMP) and phases
HA), separately for the two grains denoted 1 and 2, respectively: in the upper
the left grain is excited, in the lower row, the right one. The reconstructed
plitudes of the reflections can directly be interpreted as bright and dark-field
ages of the grain boundary.

Fig. 2 shows one sideband of the Fourier spectrum of the experimental holo-
m ((a), selection on the left hand side) of a Σ=13 (100) tilt grain boundary
gold ($\theta = 22.6^o$, see (Orchowski et al. (1995), Orchowski and Lichte (1996))
l preliminary common work (Orchowski et al. (1993))) and the reconstruc-
n (b,c) of the single reflections as indicated in the spectrum of the hologram
ered through a Gaussian mask. The upper rows (b) show modulus (AMP)
l phases (PHA) of the particular reflections chosen of types 000, {002}, and
0}, thus presenting the reconstruction of the corresponding amplitudes $\phi\mathbf{g}$

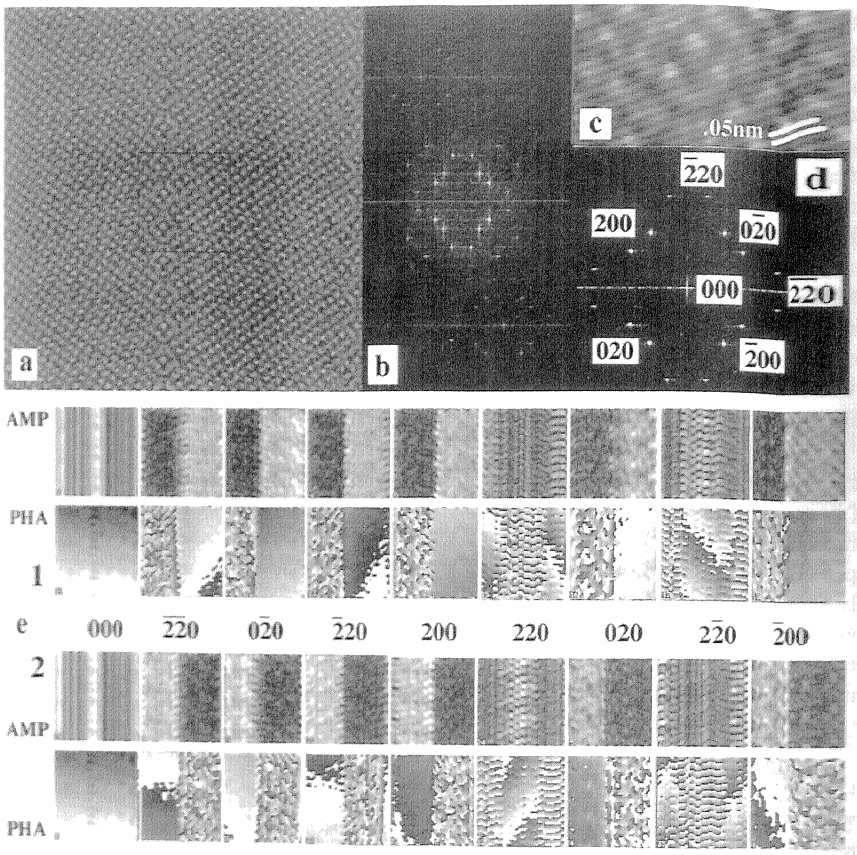

Fig. 1. Reconstruction of single reflections of a simulated MD-relaxed Σ=13 (100) Au grain boundary: (a) Theoretical hologram with the grain boundary vertically arranged in the centre, (b) Fourier spectrum of the hologram, (c) Enlarged selection of the hologram, (d) Sideband applied for reconstruction with indices of the reflections, (e) Reconstructed moduli (AMP) and phases (PHA) of the reflections of grains 1 and 2, resp.

out of the hologram. For comparison in the lower rows (c) the corresponding real (REA) and imaginary part (IMA) of the reconstructed $\phi_{\mathbf{g}}$ are presented yielding the same information, however, without the phase wrapping problem according to the multi-valued phases. The reconstruction of the higher-order reflections is impossible here because of the lower intensity of the latter and the mutual overlap of the autocorrelation and the side-band. The single reflections are denoted by 1 and 2 according to grain 1 and 2, respectively. The shift of the fringes at the grain boundary directly indicates the phase shift owing to the crystal defect. The modulation by lower frequencies is due to the local bending of the sample or to thickness oscillations.

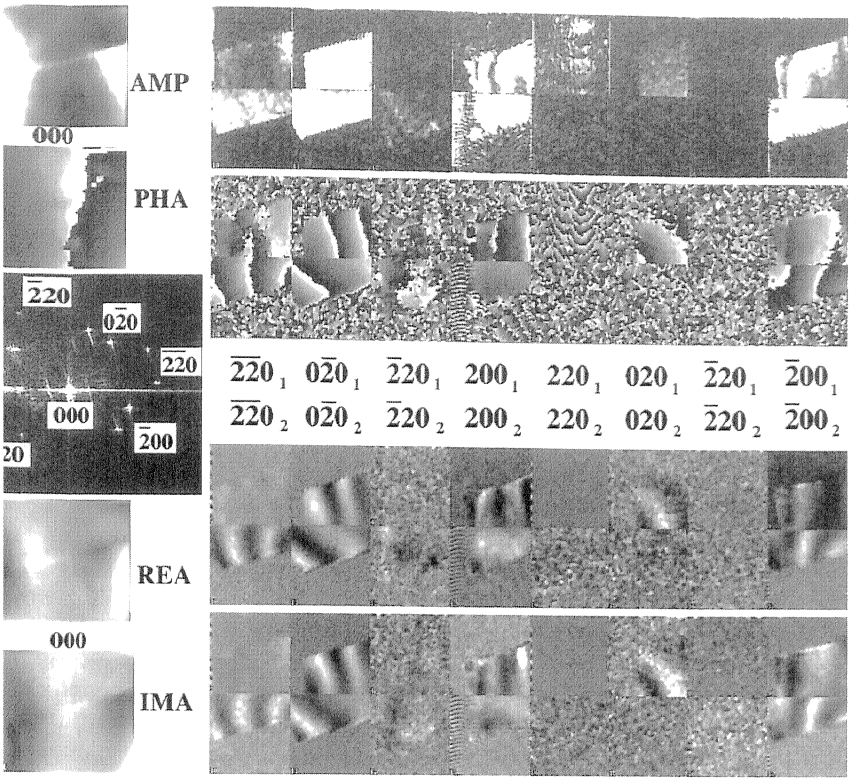

.2. Reconstruction of single reflections of a Σ=13 (100) Au grain boundary, sepely for both grains denoted by 1 and 2, respectively: (a) Fourier spectrum of the gram (0.05 nm fringes, A. Orchowski, University Tübingen (Orchowski and Lichte 6), Orchowski et al. (1993))), with indicees of the reflections and asymmetric inities in the sideband showing the mistilted orientation, (b) reconstructed moduli IP) and phases (PHA), (c) reconstructed real (REA) and imaginary (IMA) part of partial waves.

Inversion by linearization and discretization

(2) can be linearized applying perturbation methods. Assuming that the nvalues γ are non-degenerated, and by analogy with eq. (3), the perturbation ition may read

$$\Phi = \Gamma \Xi \Gamma^{-1} \theta, \tag{6}$$

where the matrices are given by

$$= C(1+\Delta), \Xi = \{e^{2\pi i \lambda t}\}, \text{ and } \lambda = \gamma + \Delta\{\delta_{ij}\} + \Delta^{-1}\{1/(\gamma_i - \gamma_j)\}\Delta. \tag{7}$$

As diagonal elements the perturbation matrix $\Delta_{\mathbf{gh}} = (\Delta\mathbf{K}.\mathbf{g}) + \mathbf{i}\Delta\mathbf{V}_{\mathbf{gh}}$ conis the deviation of the orientation $\Delta\mathbf{K}$ from that of the original eigenvalue

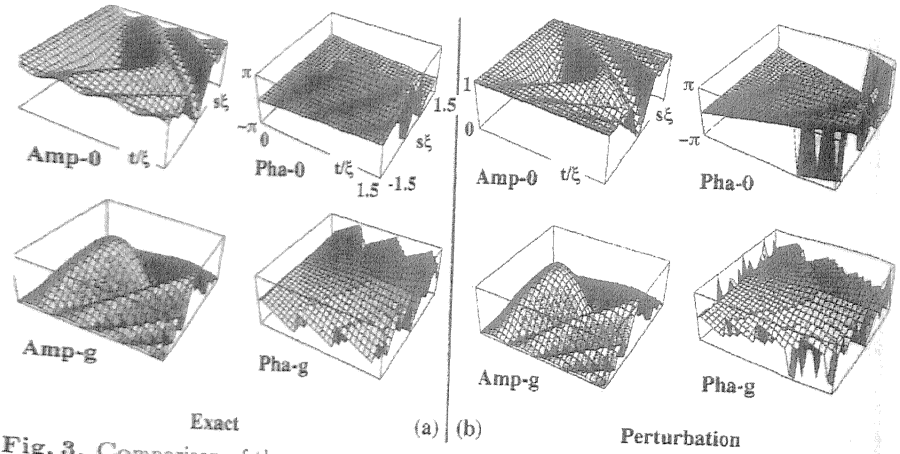

Fig. 3. Comparison of the exact two-beam solution (a) of moduli (AMP) and phases (PHA) of transmitted (0) and diffracted beam (g) with the corresponding perturbation solution (b). Differences occur for orientations with $|s\xi| > 1$, e.g., where the perturbation is no longer valid (s=Bragg deviation, t=crystal thickness, ξ=extinction distance).

system $\mathbf{K}$. The non-diagonal elements describe a perturbation of the potential as, e.g., according to optical absorption. Fig. 3 demonstrates the validity of the perturbation solution comparing eq. (6) with the exact solution (3) of the two-beam case. As for moduli and phases, for both reflections there are remarkable deviations for $|s\xi| > 1$ almost independent of thickness t around the exact orientation of the pole $|s\xi| = 0$ of the exact two-beam excitation.

Starting from approximate values of thickness t_o and beam orientation (k_{x_o}, k_{y_o}) gained from a priori knowledge or by analysing, e.g., the asymmetry of the single reflections reconstructed from the holographically retrieved wave function, the perturbation solution is valid within certain intervals around t_o and (k_{x_o}, k_{y_o}). Eq.(6) can be expanded in a Taylor series yielding

$$\phi(t, k_x, k_y) = \phi(t_o, k_{x_o}, k_{y_o}) + (t - t_o)\partial\phi/\partial t + (k_x - k_{x_o}, k_y - k_{y_o})\nabla_k\phi. \quad (8)$$

The derivatives can directly be gained from eqs. (8) using equivalent abbreviations:

$$\partial\phi/\partial t = \Gamma\partial\Xi/\partial t\Gamma^{-1}\theta \text{ and } \nabla_k\phi = (\nabla_k\Gamma\Xi - \Gamma^{-1}\nabla_k\Gamma\Xi + \Gamma\nabla_k\Xi)\Gamma^{-1}\theta \quad (9)$$

The linearized eq.(8) together with the analytical expressions (9) enable the inverse solution:

$$(t, k_x, k_y) = \mathbf{M_{inv}}[\phi^{\mathbf{exp}} - \phi^{\mathbf{pert}}], \quad (10)$$

where the matrix is given, e.g., by the Penrose-Moore inverse $\mathbf{M_{inv}} = (\mathbf{M^T M})^{-1}\mathbf{M^T}$, which is represented analytically using the matrix of the coefficients $\mathbf{M} = (\partial\phi/\partial t, \nabla_{\mathbf{k}}\Phi)$ of eq.(9). ϕ^{exp} are the measured data and ϕ^{pert} the

ion of the perturbation equation (6) at t_o, K_o. The series expansion (8) as as the resulting formalism (9) can be extended to include also the derivatives viations from potential coefficients, which are omitted here for the sake of licity. That means, additional unknown object parameters can be included e retrieval procedure as far as the problem remains overdetermined with ct to the unknowns.

lgorithm (10) is the solution to the inverse problem concerning the local ness and orientation analysis, the regularized inverse iteration can directly plied to each pixel in the real space representation of the single reflections structed from the hologram. On the suitable assumption of the basic eigen- system (2) and starting with suitable local thickness t_o as well as incident orientation (k_{xo}, k_{yo}) the values of thickness t and orientation (k_x, k_y) are ably enhanced if eq. (10) is applied to the amplitudes and phases measured ch image pixel and each reflection **g**.

igures 4 and 5 demonstrate the applicability using the single reflection wave struction of Figs. 1 and 2, respectively. In both cases, the same nine-beam value system was used to model the diffraction behaviour. Here, no further nption was made as to the initial thickness t_o. The best fit was revealed by hing the absolute minimum of the defect of the vector norm at an extended ness intervall. Fig. 4 results in a flat tickness t(i,j) as assumed for the ation of the corresponding hologram. The retrieved incident wave vector) shows oscillations with the pixel numbers, caused by the bending of the e planes, which results from the relaxation of the grain boundary because e additional twist component assumed. Different but small regularization neters γ (here γ=.0001 was assumed) do not smooth the noise if solely the intensity (see chapter 4) is regularized. In the case of retrieving from the imental hologram, different initial orientations of $\mathbf{K_0}$=(.51,.71,.0) in Fig. nd of $\mathbf{K_0}$=(-.28,1.21, .0) in Fig. 5b, yield very noisy results in thickness t orientation (k_x, k_y) for the 64x64 pixels retrieved. Nevertheless, both cases almost the same values t$\approx .77\xi$ and t=0 for the plateau of the object and ole, respectively.

he differential equations (4) allow the diffusion-like interpretation and can scretized using standard difference algorithms (Scheerschmidt and Knoll), Scheerschmidt and Knoll (1995a)). An algebraic equation system results, formally reads

$$\Phi(i,j,k-1) = \mathbf{F_1}\{\Phi(\mathbf{i,j,k}), \Phi(\mathbf{i \pm 1, j, k}), \Phi(\mathbf{i, j \pm 1, k}), \mathbf{v(i,j,k)}\} \qquad (11)$$

or the complex amplitudes Φ and the elastic displacements **v** at the (xyz)- points (i,j,k), (i±1,j,k), (i,j±1,k) and (i,j,k±1) representing the object. Pe- c boundary conditions are assumed in x and y direction, whereas at the exit ace, a further equation is given applying the forward integration of eq. (11) ide the crystal and discretizing the symbolic equation (5).

Within the crystal the difference equations (11) are equivalent for backward) and forward (k+1) integration with respect to the beam propagation, thus g insufficient for determining both the wave amplitudes Φ(i,j,k) and the ic displacement field **v**(i,j,k) at the grid points (i,j,k) considered. This be-

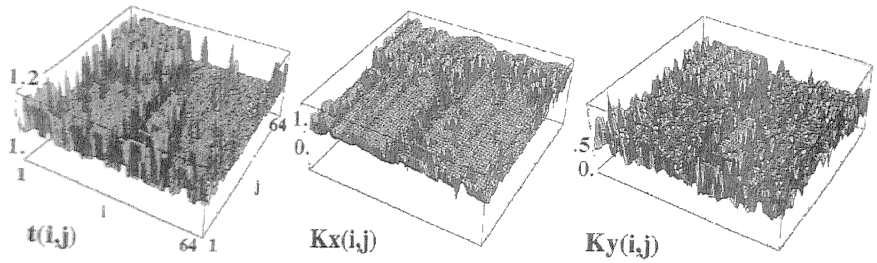

Fig. 4. Iteratively determined local sample thickness t and beam orientation (K_x, K_y) retrieved from the reconstructed reflections of the theoretical hologram in Fig. 1 for arbitrary start values of thickness and given start values of orientation without regularization.

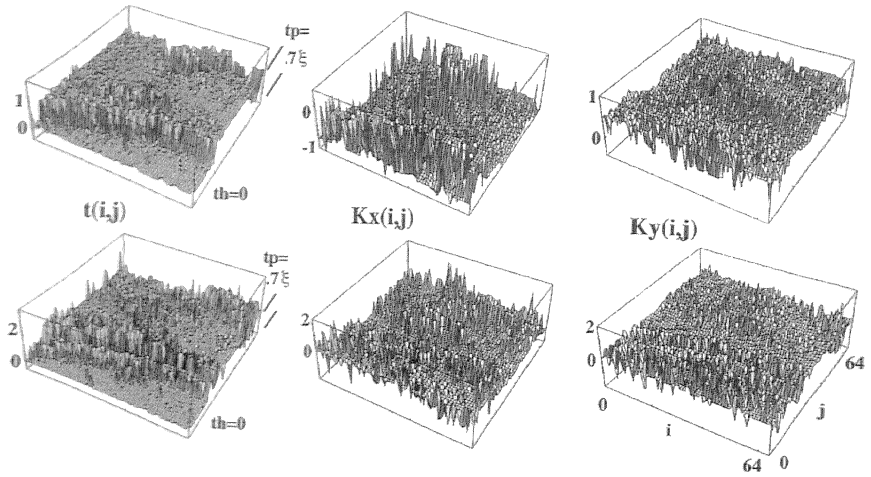

Fig. 5. Non-stabilized iteratively determined local sample thickness t and beam orientation (K_x, K_y) retrieved from the reconstructed reflections of the experimental hologram in Fig. 2 for arbitrary start values of thickness t (resulting in stable solutions th=0 in the hole, and tp $\approx .77\xi$ on the plateau) and given start values of orientation $\mathbf{K_O}$=(.51,.71,0) and $\mathbf{K_O}$=(-.28,1.21,0) for the upper and lower rows, respectively.

comes also obvious by simply numbering the unknowns and the equations at each node: for N beams, there are N unknown amplitudes and 3 unknown displacements, and N relations according to eqs. (11), using either (k-1) or (k+1). One of the difference equations, however, can be replaced as follows: While the optical potential in the reciprocal space representation is generally non-hermitian, the hermiticity of the potential V' and of the "absorption" V" yields the equation of continuity for the whole current $I = \Sigma\phi\mathbf{g}\phi\mathbf{g}^*$. The continuity equation may then read

$$\partial I/\partial z = \Phi\nabla^2\Phi^* - \Phi^*\nabla^2\Phi + 2(\mathbf{k}+\mathbf{g})\nabla\mathbf{I} - \mathbf{2\Phi V''}[\mathbf{e}^{\mathbf{igv}}]\Phi^* \qquad (12)$$

The equation of continuity can be discretized by analogy with the discretization of the differential equations above. The differential operator, however, yields mixed terms with respect to different nodes (i,j,k) and (i±1,j±1,k):

$$\mathbf{F_2}\{\mathbf{v(i,j)}, \Phi\mathbf{(i,j,k+1)}, \Phi\mathbf{(i,j,k)}, \Phi\mathbf{(i \pm 1,j,k)}, \Phi\mathbf{(i,j \pm 1,k)}\} = \mathbf{0} \qquad (13)$$

y analogy with the Gelfand-Levitan-algorithm (see, e.g., (Zakhariev and o (1990))) an additional equation results by inverting the equation of con- ty, which is a kind of completeness relation, yielding

$$\sum_{\mathbf{g}} Q_{\mathbf{g}} e^{2\pi \mathbf{g v}} = 0 \qquad (14)$$

ır eq. (13) as well as for the additional boundary condition previously dis- d. Coefficients $Q_{\mathbf{g}}$ are explicitely given in (Scheerschmidt and Knoll (1994)). , in principle, the retrieval of the displacements $\mathbf{v}$ is given by the remai- inverse problem (14), implying to find the root of a function given by an ıplete Fourier transform.

he inverse problem (14) is ill-posed for two reasons: Only one equation has solved for the vectorial root $\mathbf{v}$(i,j,k) at node (i,j,k), thus coplanar vectors ve one component unconsidered. The spectrum $Q_{\mathbf{g}}$(i,j,k) is incomplete and . This results in unstable numerical solutions using standard algorithms to he roots (viz. Newton-Raphson algorithm, genetic algorithms and neuronal ›rks), owing to the existence of a large number of subsidiary roots. Besides umerical solutions, transforming eq.(14) yields iterative forms as a kind of -regularization (Scheerschmidt and Knoll (1995a)), the system then refers overdetermined system in the same manner as discussed above.

Numerical aspects

inversion proposed is based on the linearization and the fact that the prob- s overdetermined with respect to the unknowns but underdetermined if the is included, resulting in a least square minimization of a suitable vector ı of the defect (Lois (1989), Bertero (1989)), e.g.,

$$||\Phi^{exp} - \Phi^{pert}|| = Min. \qquad (15)$$

s the iteration procedure seems to be amplifying the noise, the regulari- ns should be further enhanced. Simple averaging of the retrieved thicknesses orientations with values larger than a certain threshold omitted, avoids ers and leverages, however, structural details, too, thus yielding incorrect arization.

he stability of the procedure may be enhanced by using more general reg- zations as, e.g., the Phillips regularization. The most general regularization be of the Ivanov-Phillips-Tichonov-type (see, e.g., (Bertero (1989))),

$$^{p} - \Phi^{pert}||^2 + \gamma||Z||^2 = (\Phi^{exp} - \Phi^{pert})^{\dagger} C_1 (\Phi^{exp} - \Phi^{pert}) + \gamma Z^T C_2 Z = Min \qquad (16)$$

/hile the Moore-Penrose inverse minimizes the defect, an additional con- ıt here allows one to weight the measured data by C_1 and to smooth the ion $Z = (t, k_x, k_y)$ by C_2. Using the Moore-Penrose or similar general- ›ns always allow ill-posed problems with discrete data to be transformed

to well-posed, but mostly ill-conditioned, problems: The solution exists and is unique, however, mostly unstable. The generalized solution may be considered an average of the true solutions, the resulting generalized inverse including the regularization matrices may be

$$M_{inv} = (M^{\dagger} C_1 M + \gamma C_2)^{-1} M^T \qquad (17)$$

with the suitable regularization factor γ and matrices C_1 and C_2, respectively. The iterative solution of eq. (11) with this generalized inverse (17) yield a self-consisting approach.

The generalized approach represents the maximum-likelihood solutions if the weight matrizes C_1 are suitably chosen with respect to the reflections **g**. Gaussian distributed noise can be described by unit weights, Poisson distributed noise demands weights inversely proportional to the intensity of the reflections.

In image processing, however, the regularization is described as a procedure smoothing the pixels (i,j) (Huang (1975)) : A solution with small second derivatives with respect to neighbouring pixels tends to be more accurate. In general, any constraint C_2 which is quadratic (Huang (1975)), may be used to yield a solution resembling eqs.(10) and (17).

Assuming that the different weights can be separated without a loss of generality, the weighting C_1 is given by $W_{\mathbf{gh}}{}^{\dagger} W_{\mathbf{g'h'}}$ with W$\sim |\Phi|^{\rho}$. The smoothing C_2 can be described by matrix filters with respect to the pixels (i,j). A zero-order smoothing is equivalent to outlier detection or avoiding levarages (Rousseeuw (1977)).

The regularization parameter can be bounded (Bertero (1989)), but in the physically relevant problems such bounds are too rough and should be estimated by numerical tests. To study the confidence level of the solutions the retrieved thicknesses and orientations are compared with those used in simulated holograms, which have been performed for either perfect crystals with increasing thickness and linearly varying orientation, or for the theoretical grain boundary of Figs.1 and 4 relaxed by molecular dynamics. To check the reliability and accuracy by using simulated inputs is advantageous as one can directly compare well-known numbers and thus find out the regularization parameter for the best fit. One can use different distance measures like the squared differences or the regression coefficient $r = cov(Z_{retrieve}, Z_{theory})/(\sigma_{retrieve}\sigma_{theory})$ assuming a linear hypothesis for the fit, a χ^2 test or cross correlations. Robust measures are very fast and stable: the simple sign test $s_1 = \Sigma sgn(Z_{ij} - < Z >)/N < 1$ of all pixels or the product s_2 of neighbouring pixels, for instance allow one to detect sytematic errors, whereas weigths which are controlled by the regression coefficient between retrieved and exact data (Rousseeuw (1977)) enable the finding of outliers and leverages. No test may be considered to be perfect or superior, because always a large number of differences is reflected by only one number. Fig. 6 shows in (a) the regression coefficient r, the sign tests s_1, s_2, and different $\log(\chi^2)$ measures as function of testparameters (χ_1 from the convergence error of the retrieval procedure, χ_2 with and χ_3 without outlier detection). Figs. 6(b) and (c) represent the same $\log(\chi^2)$ measures as function of the regularization parameter γ without and including pixel smoothing, respectively, i.e. (b) with $C_1 = C_2 = I$ and (c) smoothing of the second derivative

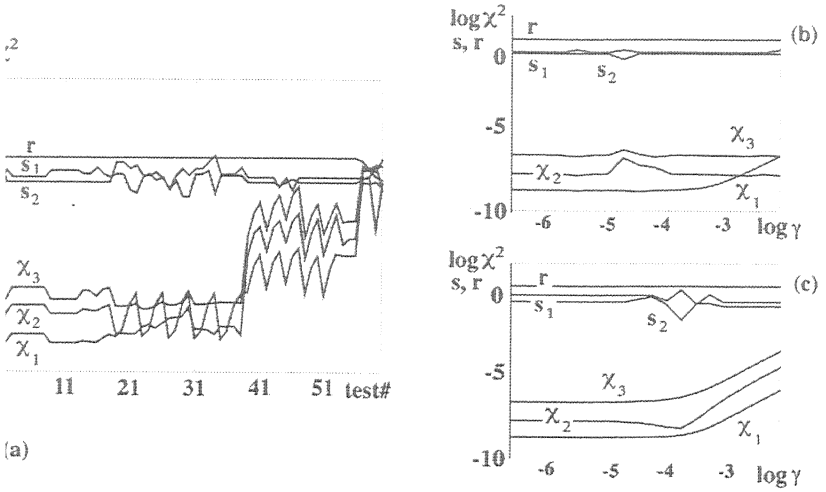

3. Confidence tests for different measures (regression r, sign tests s_1, s_2 and $\log(\chi^2)$ rieved versus simulated data as function of test parameters (a, see text) or as ion of the regularization parameter γ: (b) no smoothing $C_1 = C_2 = I$ and (c) thing of the second derivative $C_1 = I, C_2 = (\delta_{i-i_o\pm1,j-j_o\pm1} - 2\delta_{i-i_o,j-j_o})$

$C_1 = I, C_2 = [\delta_{i-i_o\pm1,j-j_o\pm1} - 2\delta_{i-i_o,j-j_o}]$. Test 1 in (a) for comparison is lated without any smoothing and normalization. The tests 2-18 are applied ormalizing the different reflexes and/or using different averages over the s and the reflexes, resp., always with $\rho = 0, \pm1, \pm2$. In the tests 19-38 addi- lly the weights C_1 are proportional to the amplitudes and intensities of the es, resp, and $\gamma = 10^{-5}, 10^{-4}, 10^{-3}, 10^{-2}$. For the test 39-53 the regulariza- s related to the a priori information instead of the maximum norm itself, $\gamma = 10^{-5}, 10^{-4}, 10^{-3}$. Clearly can be seen, that the smoothing increases rrors, whereas sytematic errors and low regression coefficients are resulting invaluable normalization. Further systematic calculations are necessary to ut the best regularization γ, i.e., the compromise between accuracy and ity of the retrieval procedure.

Conclusions

the direct solutions (11) and (12,14), i.e. the explicit evaluation of thick- nd orientation as well as the retrieval of the atomic displacements from a structed electron wave function at the exit surface of an object, result in ular inverse problems of the first kind, viz. the analysis of object parame- om measured data. Thus, from the mathematical point of view the retrieval dure is an ill-posed inverse problem requiring additional information about eriodicity of the object as the basic assumption, the thickness, the orienta- nd the unknown reconstructed displacements in order to make the process and continuous, to avoid singularities, and to restrict the manifold set of ons possible. The procedure described has transformed these difficulties to

the mathematical problem of overdetermined equation systems and of determining the roots of a function with an incomplete Fourier transform. Normalization and regularization of the solutions enable smoothing, stabilization and outlier detection.

Acknowledgements

We are grateful to the Volkswagenstiftung for financial support.

References

Anstis, G.R. (1989): Simulation techniques for reflection electron microscopy, in: Computer Simulation of Electron Microscope Diffraction and Images, Krakow, W., O'Keefe, M.A. (eds.), The Minerals, Metals and Materials Society, pp. 229–238

Bertero, M. (1989): Linear Inverse and Ill-Posed Problems, Advances in Electronics and Electron Physics **75**, 1–114

Coene, W., Janssen, G., Op de Beeck, M., van Dyck, D. (1992): Phase retrieval through focus variation for ultra-resolution in field-emission transmission electron microscopy, Phys. Rev. Letters **69**, 3743–6

van Dyck, D. (1985): Image calculation in high resolution electron microscopy: Problems, progress and prospects, in: Advances in Electronics and Electron Physics, Hawkes, P.W. (ed.), **65**, 295–355

van Dyck, D. (1989): Three-dimensional reconstruction from two-dimensional projections with unknown orientation, position and projection axis, Ultramicroscopy **30**, 435–8

van Dyck, D. , Beeck, M. Op de, Coene, W. (1993): A new approach to object wavefunction reconstruction in electron microscopy, Optik **93**, 103–7

Howie, A., Basinski, Z.S. (1968): Approximations of the dynamical theory of diffraction contrast, Philos. Mag. **17**, 1039–1063

Huang, S. (Editor) (1975), Picture Processing and Digital Filtering, Springer Vlg., N.Y.

Lavrentiev, M.M. (1967): Some Improperly Posed Problems of Mathematical Physics, Springer, Berlin, pp. 10–20

Lichte, H. (1986): Electron holography approaching atomic resolution, Ultramicroscopy **20**, 293–304

Lichte, H. (1991): Electron image plane off-axis electron holography of atomic structures, Advances in Optical and Electron Microscopy **12**, 25–91

Lichte, H. (1992): Holography - just another method of image processing?, Scanning Microscopy Suppl. **6**, 433–440

Lichte, H., Völkl, E., Scheerschmidt, K. (1991): Electron image plane off-axis electron holography of atomic structures, Advances in Optical and Electron Microscopy **12**, 25–91

Lois A.K. (1989): Inverse und schlecht gestellte Probleme, Teubner Vlg., Stuttgart

Orchowski, A., Lichte, H., Scheerschmidt, K., Scholz, R. (1993): Hochauflösende Elektronenmikroskopie zur Analyse von $\Sigma 13$ Tilt-Korngrenzen in Gold, Optik **94**, Suppl. 5, 79

Orchowski, A., Rau, W.D., Lichte, H. (1995): Electron holography surmounts resolution limit of electron microscopy, Phys. Rev. Letters **74**, 399–402

Orchowski, A., Lichte, H. (1996): High resolution electron holography of real structures at the example of a =13 grain boundary in gold, Ultramicroscopy **69**, 199–209

Rousseeuw, P.J. (1987), Robust regression and outlier detection, John Wiley & Sons, N.Y.

·schmidt, K., Hillebrand, R. (1991): Image interpretation in HREM: Direct and irect methods, Proc. 32nd Course Int. Centre of Electron Microscopy "High-olution Electron Microscopy - Fundamentals and applications", Heydenreich, J., ımann, W. (eds.), Halle, p. 56–65
·schmidt, K., Knoll, F. (1994): Retrieval of Object Information from Electron raction, I. Theoretical preliminaries, phys. stat. sol. (a) **146**, 491–502
·schmidt, K., Knoll, F. (1995): Retrieval of atomic displacements from recon-ıcted electron waves as an ill-posed inverse problem, Proc. Int. Workshop Elec-ı Holography, Knoxville Tennessee USA 1994, Tonomura, A., Allard, L.F., Pozzi, Joy, D.C., Ono, Y.A. (eds.), Elsevier Science , p. 117–124
·schmidt, K., Knoll, F. (1995): Zur Rekonstruktion von Verschiebungsfeldern aus tronen-holographisch ermittelten Objektwellen , Optik **100**, Suppl. 6, 50.
·schmidt, K. (1997): Direct retrieval of object information from diffracted electron es, Proc. 15 Pfefferkorn Conf. on Electron Imaging and Signal Processing, May 22, 1996, Silver Bay, N.Y., Scanning Microscopy Suppl. **11**, submitted
e, J.C.H., Zuo, J.M. (1992): Electron Microdiffraction, Plenum Press, New York, 134–5
ıov, A.N., Arsenin, Y.Y. (1977): Solutions of Ill-Posed Problems, Wiley, New k, pp. 1–30
riev, B.N., Suzko, A.A. (1990): Direct and Inverse Problems, Springer Vlg., Bln.-delbg.